Volume 1 | Number 1 | Jan 2013 | Pages 1–100

Journal of
Materials Chemistry A

Materials for energy and sustainability
www.rsc.org/materialsA

Li⁺

ROYAL SOCIETY OF CHEMISTRY

ROYAL SOCIETY OF CHEMISTRY

www.rsc.org/materialsA

Journal Name

ARTICLE

Large zT enhancement in hot forged nanostructured p- type $Bi_{0.5}Sb_{1.5}Te_3$ bulk alloys

Qinghui Jiang[a], Haixue Yan[a], Jibran Khaliq[a], Huanpo Ning[a], Salvatore Grasso[a], Kevin Simpson[b], Mike J. Reece[a]

Bi_2Te_3 based alloys play a dominant role in commercial applications in the fields of thermoelectric energy generation and solid state cooling. By combining the densification of nanostructured powders followed by a two-step hot forging process, hierarchical nanostructured p-type $Bi_{0.5}Sb_{1.5}Te_3$ alloys with good preferred orientation were successfully fabricated. The Seebeck coefficient in the direction perpendicular to the pressing force, which is highly anisotropic, is much greater than that of the material sintered via one-step sintering. Meanwhile, the nanostructure and crystal defects produced during hot forging also contribute to both higher Seebeck coefficient, and lower thermal conductivity due to more effective and preferential scattering of phonons than electrons. As a result, a 50% enhancement of ZT value (from 1 to above 1.5) in the orientated, hierarchical, nanostructured alloys was obtained.

1 Introduction

Thermoelectric (TE) materials and devices have received increasing attention [1] because of their potential applications in the fields of energy generation and solid state cooling.[2] Progress in this area will lead to energy systems that are less expensive and more efficient, which can contribute to solving the world's demands for energy and global climate protection. So far, many commercial uses have been realized. The efficiency of actual TE devices is determined by the TE figure of merit, $zT=(S^2\sigma/k)T$ of the materials, where S is Seebeck coefficient, σ is electrical conductivity and k is thermal conductivity.[3] There have been persistent efforts to improve zT values since the 1950s, and bulk materials with improved zT, such as PbTe,[4] LAST,[5] and skutterudites,[6] are ideal for high-temperature operations. While at close to room temperature (0° to 250°C), Bi_2Te_3 based alloys still dominate commercial applications.[7]

High zT requires high Seebeck coefficient, high electrical conductivity but low thermal conductivity. Theoretical predictions have shown that nanostructuring reduces the thermal conductivity by the selective scattering of phonons as a result of a much higher density of grain boundaries.[8] Many research groups[9, 10] have developed novel methods to synthesize nanostructured TE materials as a means to lower the thermal conductivity of the system and improve zT (>1).[11] Nanostructured isotropic bulk Bi_2Te_3-based materials can be fabricated via ball milling of melt ingots or chemical synthesis followed by spark plasma sintering or hot pressing. The lower thermal conductivity in nanostructured alloys comes from a large reduction in the phonon thermal conductivity.[9] On the other hand, because of anisotropic thermal and electronic transport properties in layer-structured materials, the zT value can be enhanced by controlling the crystallographic orientation.[12] For example, dense polycrystalline Bi_2Te_3-based alloys fabricated by slip casting,[13] hot pressing,[14] spark plasma sintering(SPS),[15-21] and melt-spinning[22, 23] methods have higher zT value because of the structural anisotropy of Bi_2Te_3. Recent research has focused on the fabrication of nanostructured Bi_2Te_3-based alloys and the size dependence of their thermoelectric properties. [19, 24-26] In this paper, high energy ball-milling was used for the preparation of the nanopowders, SPS technology was used for powder consolidation, and hot forging was used to realize hierarchical nanostructured $Bi_{0.5}Sb_{1.5}Te_3$ (BiSbTe) alloys with preferred orientation. A 50% enhancement of zT value was obtained by combining higher Seebeck coefficient from the texturing with lower thermal conductivity from the hierarchical nanostructure[27] and defects introduced during the hot forging process.

2 Experimental

To prepare alloyed nanostructured powers, appropriate amounts of the pure element bismuth, antimony, and tellurium powders were weighed according to the stoichiometry of $Bi_{0.5}Sb_{1.5}Te_3$, and poured into sealed zirconia milling pots. The powders were handled in a glove box (Ar_2 atmosphere). Nano powders were prepared using high-energy ball-milling machine (Fritsch's P7, German) at 800 rpm for 20 hours. The commercial micro-size powder was prepared by ball milling a BiSbTe ingot for 1 hour and sieving (150 mesh) the powders.

The samples were loaded into a graphite die and sintered in a SPS furnace (FCT, Germany) at a rate of 50 °C/min in a vacuum. In order to check the shrinkage rate during the SPS sintering process, we first performed a preliminary sintering run. The powder samples (micro-size and nano-size) were

heated under a constant uniaxial compressive stress of 16 MPa to a maximum sintering temperature of 450 °C. In order to investigate the plastic processing of bulk BiSbTe from nano powders below its melting point, the sample sintered at 450 °C for 5 min with diameter of 15mm was then put into a larger graphite die (25mm) and heated under a constant uniaxial compressive stress of 16 MPa to 500 °C. Having identified optimized sintering parameters, we fabricated samples with preferred orientation via a Two-Step hot forging as follows. First, two nanopowder samples were sintered at 330 °C for 20 minutes or 450 °C for 5 minutes under 50 MPa in the die (inner diameter 15 mm). Then bulk samples sintered at 330 and 450 °C were put into the center of a larger graphite die (inner diameter 25mm) and sintered at 450 and 520 °C under 50 MPa for 5 minutes, respectively.

The grain orientation was characterised using X-ray diffraction (XRD, Siemens D5000, Karlsruhe, Germany). The microstructures of the samples were observed using scanning electron microscopy (SEM, FEI, Inspect F, Hillsboro, OR) and transmission electron microscopy (TEM, JEOL 2010). The microstructure-dependent thermoelectric properties were also characterised. The samples were cut into $2.5*2.5*14$ mm^3 bars for electrical resistivity and Seebeck coefficient measurement (the long side of the bar was perpendicular to the pressing direction) using a temperature differential and four point probe methods in lab-made apparatus in a vacuum.[28]Electric and thermal transport properties were measured in the same direction. A thin slice with the thickness of 2 mm was cut from the sample parallel with the pressing direction, machined into a disk with the diameter of 10 mm, and then thermal diffusivity was measured using the laser flash method (NETZSCH, LFA457, Germany). The density (d) of the samples was measured using the Archimedes method. The specific heat was determined using differential scanning calorimetry (NETZSCH DSC 404C Germany). The thermal conductivity (k) was calculated from the product of thermal diffusivity, specific heat and density.

3 Results and discussion

Fig. 1 shows the shrinkage rates of BiSbTe micro/nanopowders /bulk during the SPS process at 16 MPa. We chose two different precursor powders to check the shrinkage rate during the densification process in order to understand the different sintering behaviour of nano-size and micro-size BiSbTe powders. The peak of the shrinking rate indicates the beginning and termination of the densification process accompanied by the elimination of pores. For the micro-size powders, there is one peak between 250 °C and 410 °C, which shows the densification stops at about 410 °C and the grains begin to grow. This is why most Bi_2Te_3 compositions are sintered at ~450 °C by SPS and achieve high densities of nearly 99%.[21, 23, 29-31] For the nanopowders, there is a broad shrinkage peak from 80 °C to 330 °C, which means the nanoparticles are more sinter active and have a wide particle size distribution. We focus on the nano-size particles in the following discussions, and a sample sintered at 330 °C for 20 min with relative density of 96%. In order to investigate the effect of plastic deformation on the properties of bulk $Bi_{0.5}Sb_{1.5}Te_3$, the sample obtained by sintering the high energy ball milled powders at 450°C for 5 min (diameter of 15 mm) was put into a larger graphite mould (25 mm) and sintered up to 500 °C under a pressure of ~16 MPa (Fig. 1c). The plastic deformation of bulk $Bi_{0.5}Sb_{1.5}Te_3$ begins above 300 °C (Stage 2, as shown in the inset of Fig. 1).

When the temperature reached 425 °C, the BiSbTe filled the graphite die and the shrinkage stopped (Stage 3).
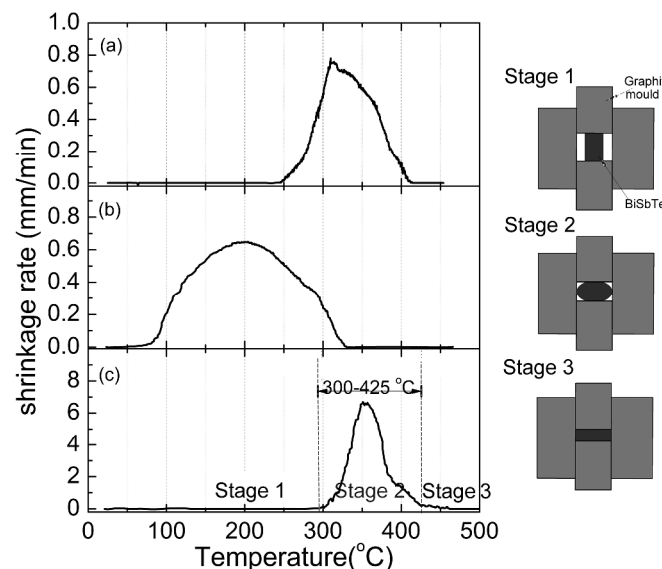
Fig. 1 The sintering behaviours of BiSbTe: (a) micro-size powders via ball milling ingot (200 rpm); (b) nano-size powders prepared via high-energy ball milling (800 rpm); (c) hot forging the sample sintered via SPS at 450 °C. (heating rate: 50 °C; pressure: 16 MPa). The left inset is the schematic during the processing in (c).

Fig. 2 shows SEM micrographs of $Bi_{0.5}Sb_{1.5}Te_3$ samples prepared under different sintering conditions. The nanopowder sintered at 330°C for 20 minutes produced samples with a density of 96% and the particle size was still in the nanometer range (50~300 nm) (Fig. 2(a)). The nanopowder sintered at 450 °C for 5 minutes produced samples with a density of 99% and randomly oriented, flake-like grains with dimensions of several μm, as shown in Fig. 2(b). This means that rapid anisotropic
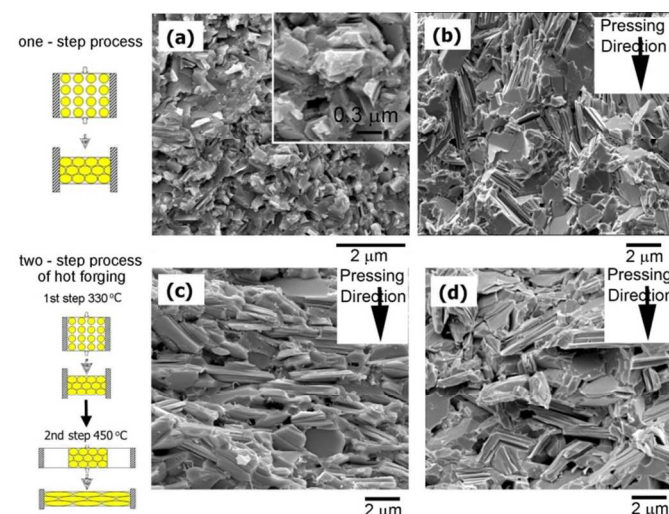
Fig. 2 SEM micrographs of $Bi_{0.5}Sb_{1.5}Te_3$ samples prepared with different sintering conditions.
(a). one step sintering at 330 °C; (b). one step sintering at 450 °C; (c). two step sintering at 330 °C and 450 °C; (d). two step sintering at 450 °C and 520 °C.

grain growth occurs above the onset temperature of grain growth (~330 °C) and there is no preferential orientation formed in the samples with one step sintering. However, during hot forging, the combination of rapid anisotropic growth and rapid superplastic deformation[32] can lead to effective grain alignment. Nano-sized grains (Fig. 2(a)) became elongated micro-sized flakes, well aligned perpendicular to the pressure's direction (Fig. 2(c)). When the grains are micro sized flakes after the first step of the sintering, the rapid deformation during the second sintering step does not produce good grain orientation, as shown in Fig. 2(d).

The crystallographic orientation of the samples was estimated using to the XRD patterns. The Lotgering factor (LF) was used to quantify the degree of preferred orientation of the (00l)-planes.

$$LF = \frac{P - P_0}{1 - P_0} \quad (1)$$

$$P_0 = \frac{I_0(00l)}{\sum I_0(hkl)}, P = \frac{I_0(00l)}{\sum I(hkl)} \quad (2)$$

where I(hkl) and I_0(hkl) are the peak intensities for measured and randomly oriented samples, respectively. Fig. 3(a) shows the XRD pattern of $Bi_{0.5}Sb_{1.5}Te_3$ samples sintered using the nanopowders prepared at 330 °C for 20 minutes under 50 MPa. All the peaks can be indexed as $Bi_{0.5}Sb_{1.5}Te_3$ with PDF card No.85-4039, which indicates that high energy ball milling plus SPS process can be used to synthesize single phase nanopowders.[33] However, a second phase was observed in the sample sintered in one step at 450 °C, as shown in Fig. 3(b). Fig. 3 (c) and (d) show the XRD patterns of the BT 450-520 sample (sintered at 450 °C and hot-forged at 520 °C) and BT330-450 sample (sintered at 330 °C and hot-forged at 450 °C), in which (00l) peaks have similarly higher relative intensity for hot forged samples. According to Eq (1), the values of LF =0.31, and 0.26 were obtained for BT330-450 and BT 450-520, which are much higher than those reported by others.[17, 18] However, there are obviously different micro morphologies according to the microstructure in Fig 2 (c) and (d). This indicates the result of XRD may not be an effective method for characterizing the preferred orientation of Bi_2Te_3 based materials. In Fig. 3 (b) and (d), there is one peak which does not belong to the $Bi_{0.5}Sb_{1.5}Te_3$ phase. It is difficult to identify this compound from a single XRD diffraction peak, however the strongest reflection of Te is found at around 27.6 ° and it matched with the pattern in Fig 1 (d). The presence of tellurium was also confirmed by TEM as reported by *Poudel B et al.*[9] Since all four samples in Fig. 3 are from the same powders, the second phase of the BT 330-450 was produced during the second sintering step. The sample with two step processing at 330 °C to 450 °C has 4% porosity. Puneet P *et al*[25] that electric currents might generate high local temperature zones from the plasma discharge in the gaps which lead to spark-plasma-sintering-induced interface modifications during the hot forging process. This might lead to the formation of low-melting-point tellurium second phase near the grain boundaries, as shown in the inset of Fig. 3. For the BT 450-520 sample, the higher processing temperature can promote diffusion between the tellurium phase and Bi-Sb-Te phase. Meanwhile, there is significant volatilization of tellurium. These events lead to the volatilization of Te again when the sample is sintered at higher temperature.
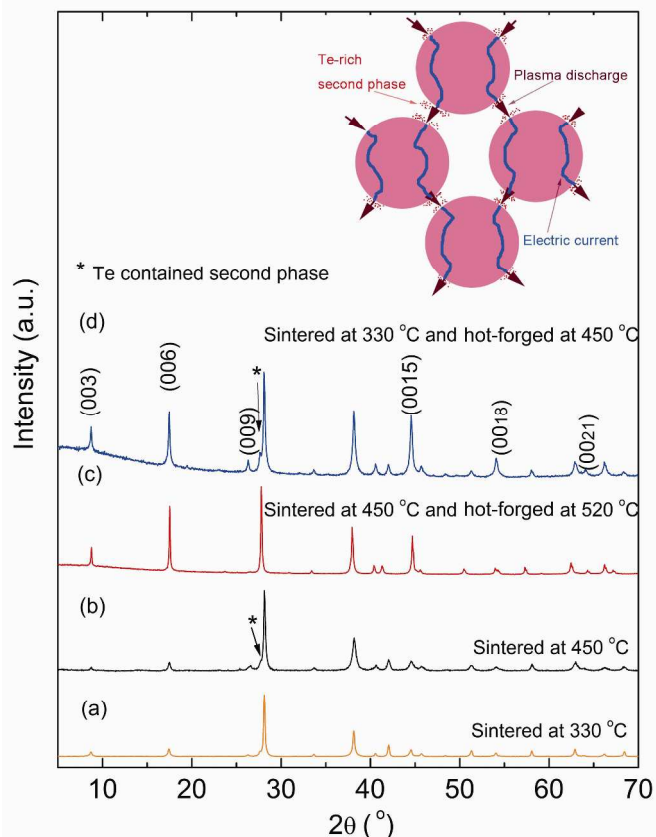
Fig. 3 XRD patterns of $Bi_{0.5}Sb_{1.5}Te_3$ samples prepared by one-step sintering (a, b) and two-step process (c, d) (the scanning surface is perpendicular to the SPS pressing) from the nano-size powders. The inset is the diagram on how the second phase might have formed.

Fig. 4(a) shows the morphology of one flake's fracture surface at high magnification in the BiSbTe sample 330-450. A flake-like grain consists of many parallel nanoflakes with thickness of 20-40 nm. These nanoflakes can be seen at higher resolution in the TEM image shown in Fig. 4(b). Fig. 4(c) shows a similar area at much higher resolution. It shows many closely packed nano-sized grains with diameter of ~10 nm. These nanograins are highly crystalline, as shown in the inset. Fig. 4(d) illustrates the hierarchical structure of the samples before and after hot forging. The densification of nano sized grains (~10 nm) prepared via the high energy ball milling process are realized via SPS process at 330 °C, and during this process larger particles with diameter of 50-300 nm appears in order to reduce the interfacial energy. Due to the rapid densification process within several minutes, there is not enough time and energy for the nano-size grains to align in one direction and grow bigger. During the hot forging process, rapid superplastic deformation can lead to the sliding and alignment of the nanograins perpendicular to the pressing direction (which can be confirmed by Fig. 4(c)). Another trend is the rapid anisotropic growth in the a-b plane of Bi_2Te_3, which leads to a hierarchical microstructure. The optimised sintering temperature and rapid densification process result in the existence of nanoparticles with diameter of ~10 nm at the bottom level. There are many nanoflakes with thickness of several tens of nanometers at the intermediate level (which is confirmed by Fig. 4(a)). At the top level, flakes with the length of several micrometres can be confirmed by Fig. 2(c).
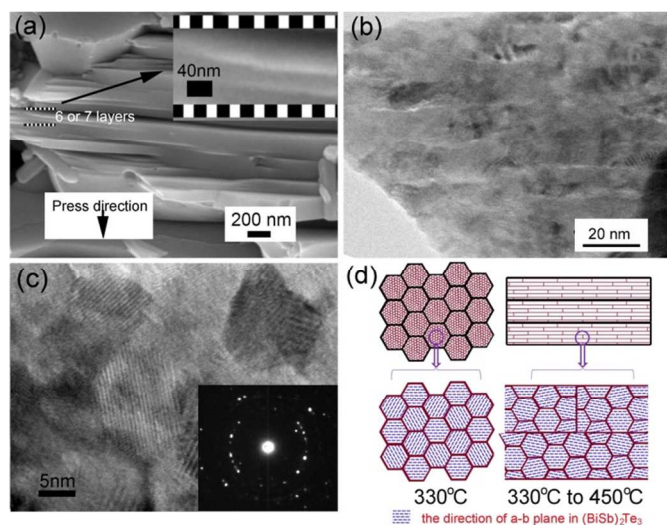
Fig. 4 SEM morphology (a), and high-solution TEM images (b) & (c) of $Bi_{0.5}Sb_{1.5}Te_3$ sample 330-450. (d) microstructural diagrams of the samples before and after hot forging.

Bi_2Te_3 has a layered structure, where five layers of Te(1)-Bi-Te(2)-Bi-Te(1) making up its the periodic structure along its c axis. Although some groups[31, 34] claim that no obvious difference was observed between the in-plane and out-of-plane zT, some groups[24, 30, 35] reported a slightly-higher zT value along the in-plane direction. ZT enhancement has already been realized in n-type Bi_2Te_3 alloys by SPS texturing.[20] Therefore, in this paper we only focused on the in-plane properties perpendicular to the pressing direction in p-type Bi_2Te_3 alloys. The Seebeck coefficient at room temperature should be sensitive to the band structure near the Fermi level, E_F, and independent of the grain orientation according to the current theory and Mott equation.[36] However, Nassary M M *et al* prepared Bi_2Te_3 single crystal by a modified Bridgman method and experimentally proved that the Seebeck coefficient of p-type materials has anisotropic nature and the value along the in-plane direction is five times larger than that along the cross-plane direction in the appropriate temperature range.[37] Two-Step hot-forging 330-450 in SPS increases the Seebeck coefficient because of good orientation in the in-plane direction, as shown in Fig. 5(a). Meanwhile, hot-forging introduces crystal defect (such as point defects, dislocations), which leads to an increase of the resistivity (Fig. 5b),[18] which should be lowest perpendicular to the pressing direction. The crystal defects may suppress the excitation of the minority carrier (electron) which leads to the maximum value of the Seebeck coefficient at 50 °C.[38] Zhao LD *et al* also reported this sudden change in Seebeck coefficient with temperature of hot forged samples as being produced by a lower carrier concentration.[20] As a result, the sample prepared with 330-450 processing temperatures had a much higher Seebeck coefficient (~300 μV/K) than the sample sintered at 450 °C (200~220 μV/K), which leads to its higher power factor. At 50 °C, the maximum value of power factor is about 5000 μW/mK², which is slightly higher than the value of bulk BiSbTe alloys prepared via hot press method[9] We used similar sintering conditions in one-step sintering, and the power factor is about 3000 μW/mK).

The thermal conductivity data of the samples sintered at 450 °C via different processes are shown in Fig. 6(a). A Lorenz number
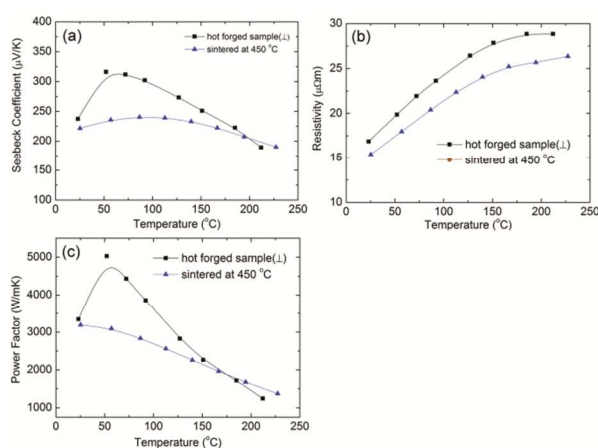
Fig. 5 Temperature dependence of Seebeck coefficient, resistivity and power factor of hot forged (330-450) sample (perpendicular to the pressing direction) compared with sample sintered at 450 °C.

of $2.45*10^{-8}V^2K^{-2}$ in the Wiedemann-Franz law ($k_e=L_0\sigma T$) was used to estimate the charge carrier contribution to the thermal conductivity.[1] Compared with the sample directly sintered at 450 °C, the hot forged sample with preferred orientation has higher thermal conductivity (8.6% for k_{total}, and 25% for k_{latt}) due to good grain orientation. The k_{latt} value is about 0.6 W/mK, which is similar to the values for other nanostructured alloys at 50 °C, as shown in Table 1. But the value measured in this work is that of the textured samples perpendicular to the pressing direction, not the average of two directions. The real k_{latt} is much lower than that of single crystal (0.82 W/mK)[39] because of the crystal defects, nanostructure and second phase.[38] As shown in Fig. 6(b), the high ZT value (above 1.5) comes from the excellent Seebeck properties of the hot-forged sample. First principles calculation[36] shows that the in-plane and cross plane Seebeck coefficient should be identical at 300 K, and thus Seebeck coefficient will be unchanged when the samples have different orientations. At room temperature, the two samples we measured have similar Seebeck coefficient (230~240 μV/K), power factor (3200~3300 μW/mK²). The samples also have similar ZT value (~1) with Ref 40.[40] At higher temperature 50 °C, the max ZT value is ~1.5 and there is a 50% difference between random orientation and good orientation. All of this illustrates that p-type Bi_2Te_3 has demonstrated complex Seebeck properties and more accurate theory modeling is required. The point line and planar defects generated via hot forging may also affect the Seebeck coefficient, which is the reason why the samples fabricated via different methods and conditions have different Seebeck coefficient[13, 21, 23, 30, 34].
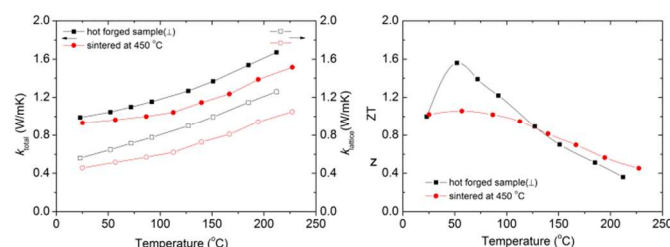
Fig. 6 Temperature dependence of thermal conductivity and zT values of the samples (perpendicular to the pressing direction)

Tab. 1 Comparison of TE parameters of selected Bi_2Te_3 simples at 50 ^oC

Type of Bi_2Te_3 sample	Power factor [mW/mK^2]	K [W/mK]	$K_{lattice}$ [W/mK]	zT	reference
$Bi_{0.5}Sb_{1.5}Te_3$ single crystal(p type)	4.8	1.51	0.82	0.94	[39] at 23 ^oC
Bi_2Te_3/Bi_2Se_3 nano composite(n type)	1.1		0.35	0.55	[26]
Melt spun BiSbTe nano composite(p type)	1.9		0.6	1.44	[23]
Nanostructure alloys(p type)	4.1	1.2		1.3	[33]
0.4%SiC doped BiSbTe nanocomposite(p type)	3.9	0.95	0.35	1.3	[19]
Hot forged BiSbTe nanostructured alloys(p type) (⊥)	5.0	1	0.6	1.56	This work

4 Conclusions

Dense, textured, nanostructured $Bi_{0.5}Sb_{1.5}Te_3$ with hierarchical structure was prepared via hot forging. The Seebeck coefficient perpendicular to the pressing direction of the hot-forged samples is much higher than for samples sintered via one-step SPS processing because of preferred orientation and boundary effects in nanostructured materials. As a result, a higher ZT value (~1.56) was obtained, which was up to 50% higher than that of samples prepared via one-step process. This study experimentally indicates that aligning the crystal orientation can enhance the performance of p- type Bi_2Te_3 nanostructure materials.

Acknowledgements

Notes

[a] School of Engineering and Materials Science, Queen Mary University of London, Mile end road, London, E1 4NS, UK. E-mail: q.jiang@qmul.ac.uk; m.j.reece@qmul.ac.uk

[b] European Thermodynamics Ltd, 8 Priory Business Park, Leicester LE8 0RX, UK

References

1. T. M. Tritt and M. A. Subramanian, *MRS Bull.*, 2006, **31**, 188-194.
2. J. R. Sootsman, D. Y. Chung and M. G. Kanatzidis, *Angew. Chem.-Int. Edit.*, 2009, **48**, 8616-8639.
3. G. Li, J. Y. Yang, Y. Xiao, L. W. Fu, J. Y. Peng, Y. Deng, P. W. Zhu and H. X. Yan, *J. Electron. Mater.*, 2013, **42**, 675-678.
4. H. Wang, J. H. Bahk, C. Kang, J. Hwang, K. Kim, A. Shakouri and W. Kim, *J. Mater. Chem. A*, 2013, **1**, 11269-11278.
5. Z. Y. Li, M. M. Zou and J. F. Li, *J. Alloy. Compd.*, 2013, **549**, 319-323.
6. S. Q. Bao, J. Y. Yang, W. Zhu, X. Fan and X. K. Duan, *J. Alloy. Compd.*, 2009, **476**, 802-806.
7. H. Y. Lv, H. J. Liu, J. Shi, X. F. Tang and C. Uher, *J. Mater. Chem. A*, 2013, **1**, 6831-6838.
8. M. S. Dresselhaus, G. Chen, M. Y. Tang, R. G. Yang, H. Lee, D. Z. Wang, Z. F. Ren, J. P. Fleurial and P. Gogna, *Adv. Mater.*, 2007, **19**, 1043-1053.
9. B. Poudel, Q. Hao, Y. Ma, Y. C. Lan, A. Minnich, B. Yu, X. A. Yan, D. Z. Wang, A. Muto, D. Vashaee, X. Y. Chen, J. M. Liu, M. S. Dresselhaus, G. Chen and Z. F. Ren, *Science*, 2008, **320**, 634-638.
10. D. G. Cahill, S. K. Watson and R. O. Pohl, *Phys. Rev. B*, 1992, **46**, 6131-6140.
11. K. Koumoto and T. Mori, *Thermoelectric Nanomaterials*, Springer Berlin Heidelberg, 2013.
12. D. L. Medlin and G. J. Snyder, *Curr. Opin. Colloid Interface Sci.*, 2009, **14**, 226-235.
13. D. H. Kim, C. Kim, D. W. Ha and H. Kim, *J. Alloy. Compd.*, 2011, **509**, 5211-5215.
14. D. H. Kim, I. H. Kwon, C. Kim, B. Han, H. J. Im and H. Kim, *J. Alloy. Compd.*, 2013, **548**, 126-132.
15. L. P. Hu, H. L. Gao, X. H. Liu, H. H. Xie, J. J. Shen, T. J. Zhu and X. B. Zhao, *J. Mater. Chem*, 2012, **22**, 16484-16490.
16. L. P. Hu, X. H. Liu, H. H. Xie, J. J. Shen, T. J. Zhu and X. B. Zhao, *Acta Mater.*, 2012, **60**, 4431-4437.
17. T. J. Zhu, Z. J. Xu, J. He, J. J. Shen, S. Zhu, L. P. Hu, T. M. Tritt and X. B. Zhao, *J. Mater. Chem. A*, 2013, **1**, 11589-11594.
18. J. J. Shen, Z. Z. Yin, S. H. Yang, C. Yu, T. J. Zhu and X. B. Zhao, *J. Electron. Mater.*, 2011, **40**, 1095-1099.
19. J. Li, Q. Tan, J.-F. Li, D.-W. Liu, F. Li, Z.-Y. Li, M. Zou and K. Wang, *Adv. Funct. Mater.*, 2013, **23**, 4317-4323.
20. L. D. Zhao, B. P. Zhang, J. F. Li, H. L. Zhang and W. S. Liu, *Solid State Sci.*, 2008, **10**, 651-658.
21. F. Li, X. Y. Huang, Z. L. Sun, J. A. Ding, J. Jiang, W. Jiang and L. D. Chen, *J. Alloy. Compd.*, 2011, **509**, 4769-4773.
22. T. S. Kim and B. S. Chun, *J. Alloy. Compd.*, 2007, **437**, 225-230.
23. W. J. Xie, X. F. Tang, Y. G. Yan, Q. J. Zhang and T. M. Tritt, *Appl. Phys. Lett.*, 2009, **94**, 102111.
24. W. J. Xie, S. Y. Wang, S. Zhu, J. He, X. F. Tang, Q. J. Zhang and T. M. Tritt, *J. Mater. Sci.*, 2013, **48**, 2745-2760.
25. P. Puneet, R. Podila, S. Zhu, M. J. Skove, T. M. Tritt, J. He and A. M. Rao, *Adv. Mater.*, 2013, **25**, 1033-1037.
26. Y. Min, J. W. Roh, H. Yang, M. Park, S. I. Kim, S. Hwang, S. M. Lee, K. H. Lee and U. Jeong, *Adv. Mater.*, 2013, **25**, 1425-1429.
27. K. Biswas, J. Q. He, I. D. Blum, C. I. Wu, T. P. Hogan, D. N. Seidman, V. P. Dravid and M. G. Kanatzidis, *Nature*, 2012, **489**, 414-418.

28. X. A. Fan, J. Y. Yang, W. Zhu, S. Q. Bao, X. K. Duan, C. J. Xiao and K. Li, *J. Alloy. Compd.*, 2008, **461**, 9-13.

29. C. Chen, D. W. Liu, B. P. Zhang and J. F. Li, *J. Electron. Mater.*, 2011, **40**, 942-947.

30. C. Euvananont, N. Jantaping and C. Thanachayanont, *Curr. Appl. Phys.*, 2011, **11**, S246-S250.

31. J. J. Shen, T. J. Zhu, X. B. Zhao, S. N. Zhang, S. H. Yang and Z. Z. Yin, *Energy Environ. Sci.*, 2010, **3**, 1519-1523.

32. Z. J. Shen, J. Liu, J. Grins, M. Nygren, P. L. Wang, Y. M. Kan, H. X. Yan and U. Sutter, *Adv. Mater.*, 2005, **17**, 676-680.

33. Y. Ma, Q. Hao, B. Poudel, Y. C. Lan, B. Yu, D. Z. Wang, G. Chen and Z. F. Ren, *Nano Lett.*, 2008, **8**, 2580-2584.

34. D. H. Kim, C. Kim, S. H. Heo and H. Kim, *Acta Mater.*, 2011, **59**, 405-411.

35. M. Situmorang and H. J. Goldsmid, *Phys. Status Solidi B-Basic Res.*, 1986, **134**, K83-K88.

36. B. L. Huang and M. Kaviany, *Physical Review B*, 2008, **77**, 125209.

37. M. M. Nassary, H. T. Shaban and M. S. El-Sadek, *Mater. Chem. Phys.*, 2009, **113**, 385-388.

38. Y. Lan, A. J. Minnich, G. Chen and Z. Ren, *Adv. Funct. Mater.*, 2010, **20**, 357-376.

39. T. Caillat, M. Carle, P. Pierrat, H. Scherrer and S. Scherrer, *J. Phys. Chem. Solids*, 1992, **53**, 1121-1129.

40. P. J. Taylor, J. R. Maddux, W. A. Jesser and F. D. Rosi, *J. Appl. Phys.*, 1999, **85**, 7807-7813.

Journal of Materials Chemistry A Accepted Manuscript